Materials and Design 53 (2014) 145–151

Contents lists available at SciVerse ScienceDirect

Materials and Design

journal homepage: www.elsevier.com/locate/matdes

Glass forming ability, thermodynamics and mechanical properties of novel Ti–Cu–Ni–Zr–Hf bulk metallic glasses

Peiyou Li [a], Gang Wang [b], Ding Ding [b], Jun Shen [a,*]

[a] School of Materials Science and Engineering, Harbin Institute of Technology, Harbin 150001, People's Republic of China
[b] Laboratory for Microstructures, Shanghai University, Shanghai 200444, People's Republic of China

ARTICLE INFO

Article history:
Received 19 March 2013
Accepted 25 June 2013
Available online 3 July 2013

Keywords:
Bulk metallic glass
Glass forming ability
Thermodynamics
Mechanical properties

ABSTRACT

Novel, pentabasic Ti–Cu–Ni–Zr–Hf bulk metallic glasses (BMGs), with critical diameters of 2–4 mm, were successfully developed through the proportional mixing of the binary eutectic compositions of $Ti_{27}Cu_{73}$, $Ti_{76}Ni_{24}$, $Zr_{76}Ni_{24}$ and $Hf_{84}Ni_{16}$. According to the concept of binary eutectic units, five Ti–Cu–Ni–Zr–Hf BMGs were fabricated, of which the $Ti_{29.44}Cu_{46.72}Ni_{7.88}Zr_{7.6}Hf_{8.4}$ alloy had the lower glass forming ability, and the smallest reduced ideal glass transition temperature δ and $\Delta C_p^m/\Delta S_m$ values, where ΔC_p^m and ΔS_m represent the specific heat and entropy differences at the melting temperature (T_m), respectively. The $Ti_{29.44}Cu_{46.72}Ni_{7.88}Zr_{7.6}Hf_{8.4}$ alloy also showed good mechanical properties, i.e., good plastic strain and relatively high compressive strength.

1. Introduction

Bulk Metallic glasses (BMGs) exhibit the excellent comprehensive properties, such as high strength, high hardness, good corrosion resistance and many others [1]. Since that, tremendous research work focus on the development of BMGs that simultaneously possess a high strength and a reasonable amount of plasticity [1]. However, searching for novel alloy compositions with high glass forming ability (GFA) is a tedious and costly process. In recent years, several characteristic, empirical parameters have been proposed as being relevant to the development of new BMGs, including: the glass transition temperature, T_{rg} ($=T_g/T_l$, where T_g is the glass transition temperature and T_l is the liquidus temperature) [2]; the supercooled liquid region, ΔT_x ($=T_x-T_g$, where T_x is the crystallization onset temperature) [3]; the γ parameter ($=T_x/(T_x+T_l)$) [4]; and the thermodynamic parameter, γ' ($=GFA \propto \Delta H^{liq}\cdot\Delta H^{amor}/(\Delta H^{inter})^2$, where ΔH^{liq}, ΔH^{amor} and ΔH^{inter} are the formation enthalpy of liquid, glasses and intermetallic compounds, respectively.), for predicting GFA in binary metallic glasses [5]. These parameters may be measured in calorimetric experiments [6]. In order to facilitate the effective design of new BMGs with high GFA, a method called "proportional mixing of binary eutectics" was developed [7,8]. The validity of this method has been verified using Zr- [7–9], Cu- [10], Ti–Zr- [5] and Ti–Cu- [11] based BMGs. It has been found that in a given alloy system, alloys with deep eutectic compositions had a high GFA [2,8,12]. Lu et al. [8] have developed the physical concept of strong clusters of binary eutectics in an ideal glass-forming liquid, to elucidate good glass-forming compositions in multicomponent systems. Based on the concept of proportional mixing of binary eutectic units, a ternary Ti–Zr–Be BMGs [6], and quaternary Zr–Al–Cu–Ni(Fe) [7–9] and Ti–Cu–Ni–Zr [10,11] BMGs have been developed. These ternary and quaternary BMGs have usually contained two or three binary eutectic units [6,7–11]. However, pentabasic alloys with more than three binary eutectic units are more useful for the exploration of new, complex compositions formed by proportional mixing of binary eutectic units [7,8].

Ti–Cu-based BMGs are of great scientific and commercial interest due to their high specific strength [12–20]. However, most currently available Ti- or Ti–Cu-based BMGs with high GFA contain Be, a poisonous element [12–14], or noble elements such as Pd [16,17], which does not meet the requirements of designing "green" or engineering materials [1]. A pentabasic Ti–Cu–Ni–Zr–Hf alloy, with a diameter of 1.5 mm, has been shown to exhibit high fracture strength [21]. Therefore, we have explored novel, glass-forming compositions of pentabasic Ti–Cu–Ni–Zr–Hf alloys, based on the proportional mixing of binary eutectic units, and investigated systematically the GFA, thermodynamics and mechanical properties of these Ti–Cu–Ni–Zr–Hf BMGs.

2. Experimental procedure

Ingots of Ti–Cu–Ni–Zr–Hf alloys were prepared by arc-melting a mixture of pure metal elements (of purity > 99.99%) in a titanium-gettered argon atmosphere. To achieve chemical homogeneity, all ingots were re-melted at least four times, and then suction-cast

* Corresponding author. Tel.: +86 451 86403195; fax: +86 451 86403196.
E-mail address: junshen@hit.edu.cn (J. Shen).

0261-3069/$ - see front matter © 2013 Elsevier Ltd. All rights reserved.
http://dx.doi.org/10.1016/j.matdes.2013.06.060

into copper molds to form rod-shaped samples with different diameters. The microstructure of each of these samples was characterized by X-ray diffraction (XRD), using a Philips X-pert system with Cu Kα radiation at 30 kV. Thermal analysis of samples with a diameter of 3 mm was carried out using a differential scanning calorimeter (DSC) and differential thermal analyzer (DTA), under continuous argon flow and at a heating rate of 0.33 K s^{-1} (Perkin–Elmer DSC 7). For each sample, the specific heat capacities of the amorphous phase, the phase in the supercooled liquid state and the crystalline phase were measured by comparison with the specific heat capacity of a sapphire standard sample.

The specific heat capacities of the amorphous phase, supercooled liquid phase, and crystalline phase were also measured on DSC-7 by comparing with the specific heat capacity of a sapphire standard sample using the following equation [22]:

$$C_p(T)_{sample} = \frac{\dot{Q}_{sample} - \dot{Q}_{pan}}{\dot{Q}_{sapphire} - \dot{Q}_{pan}} \times \frac{m_{sapphire} - u_{sample}}{m_{sample} - u_{sapphire}} \times C_p(T)_{sapphire} \quad (1)$$

where m is the mass, u the molecular weight and $C_p(T)$ sapphire the standard specific heat capacity of the sapphire. The term $\dot{Q}$ is defined as [22]:

$$\dot{Q} = \frac{dQ}{dt} = \left(\frac{\partial Q}{\partial t}\right)_{T\neq 0} - \left(\frac{\partial Q}{\partial t}\right)_{T=0} = C \cdot \frac{dT}{dt} \quad (2)$$

and the first term $(\partial Q/\partial t)_{T\neq 0}$ corresponds to the power necessary to heat the sample and its sample pan at a constant rate of 0.33 K s^{-1}, $(\partial Q/\partial t)_{T=0}$ is the power needed to hold the sample and its pan isothermally and C refers to the heat capacity of the sample and the pan. In order to identify the heat flow into the sample, identical measurements were also performed on the empty sample pan and a sapphire reference. The specific heat capacity of the samples was then calculated. The heat capacity measurements were performed at a heating rate of 0.33 K s^{-1}, using flakes of samples (6–20 mg) with a diameter of 3 mm.

Considering that BMGs usually have a small dimensional size, and the test standards, such as ASTM and ISO standards, are not suitable for the current study, we use a special test procedure to meet our BMG samples' size. A cylindrical sample, with a diameter of 2 mm and a height of about 4 mm, was prepared from the as-cast rods for uniaxial compression tests. Because our metallic glasses are very small in dimensional size, we have to use the special test procedures. The compression tests were carried out at room temperature in a SANS 1500 compression testing machine, with a strain rate of 2.5×10^{-4} s^{-1}. The quantitative data were all measured for three times, and were the average data. After compression, the fracture surfaces were investigated with scanning electron microscopy (SEM) using a Hitachi SU 1510 machine.

3. Designing pentabasic Ti–Cu–Ni–Zr–Hf alloys

Ti, Zr and Hf elements can form strong clusters of binary eutectics with Cu and Ni elements, respectively, such as TiCu, TiNi, ZrCu, ZrNi, HfCu and HfNi binary eutectic phases [8]. In addition, Ti, Zr and Hf elements can form weak clusters of continuous solid solutions, over the entire composition range, with Cu and Ni elements [8]. Based on the scheme proposed previously by Lu et al. [8], the pentabasic (Ti, Zr, Hf)–(Cu, Ni) system may be regarded as an ideal glass-forming liquid in which strong, stable clusters of binary eutectics can survive and dominate the structural behavior; weak clusters are not considered in the design of novel alloy compositions [8]. Thus, the composition, C_{am}, of good glass formers in this system may be expressed as the following:

$$C_{am} = a(\mathrm{Ti}-\mathrm{Cu}) + b(\mathrm{Ti}-\mathrm{Ni}) + c(\mathrm{Zr}-\mathrm{Ni}) + d(\mathrm{Hf}-\mathrm{Ni}) + e(\mathrm{Zr}-\mathrm{Cu}) + f(\mathrm{Hf}-\mathrm{Cu}) \quad (3)$$

where a, b, c, d, e and f are constants, and the sum of these constants is unity. The tendency for the formation of crystalline phases from the individual binary clusters correlates with their concentration and the heat of mixing [8]. As suggested in the literature, determination of the values of the constants, a, b, c, d, e and f, follows the rule that clusters with a large negative heat of mixing should have a relatively low concentration. Thus, the tendency for forming crystalline phases can be minimized. As a rule of thumb, the initial values for a, b, c, d, e and f, for a base composition, C_{base}, may be derived based on:

$$a\Delta H_{\mathrm{Ti-Cu}} = b\Delta H_{\mathrm{Ti-Ni}} = c\Delta H_{\mathrm{Zr-Ni}} = d\Delta H_{\mathrm{Hf-Ni}} = e\Delta H_{\mathrm{Zr-Cu}} = f\Delta H_{\mathrm{Hf-Cu}} \quad (4)$$

where $\Delta H_{\mathrm{Ti-Cu}}$, $\Delta H_{\mathrm{Ti-Ni}}$, $\Delta H_{\mathrm{Zr-Ni}}$, $\Delta H_{\mathrm{Hf-Ni}}$, $\Delta H_{\mathrm{Zr-Cu}}$ and $\Delta H_{\mathrm{Hf-Cu}}$ represent the heat of mixing for the atomic pairs Ti–Cu, Ti–Ni, Zr–Ni, Hf–Ni, Zr–Cu and Hf–Cu, respectively. Combining Eqs. (3) and (4), one may quickly determine the C_{base} value for good glass formation ability in the Ti–Cu–Ni–Zr–Hf alloy system.

The heats of mixing of atomic pairs among the main elements [23] in the Ti–Cu–Ni–Zr–Hf alloy system are listed in Table 1. For binary systems with a single eutectic point, their deepest eutectic points are $Ti_{27}Cu_{73}$, $Ti_{76}Ni_{24}$, $Zr_{76}Ni_{24}$, $Hf_{84}Ni_{16}$, $Zr_{38}Cu_{62}$ and $Hf_{38}Cu_{62}$. According to Eq. (4), the smaller negative heat of mixing requires a relatively larger constant. Thus, it may be determined that the contents of $Ti_{27}Cu_{73}$, $Zr_{38}Cu_{62}$ and $Hf_{38}Cu_{62}$ must be higher than those of $Ti_{76}Ni_{24}$, $Zr_{76}Ni_{24}$ and $Hf_{84}Ni_{16}$, indicating that a Cu-rich composition is desirable in the Ti–Cu–Ni–Zr–Hf system. In order to obtain a Ti–Cu-rich composition in the Ti–Cu–Ni–Zr–Hf system, the deep eutectic composition of $Ti_{27}Cu_{73}$ is retained, but the eutectic compositions of $Zr_{38}Cu_{62}$ and $Hf_{38}Cu_{62}$, with high Cu contents, are removed. Thus, a Ti–Cu-rich composition in the Ti–Cu–Ni–Zr–Hf alloy may be formulated as:

$$C_{am} = a(\mathrm{Ti_{27}Cu_{73}}) + b(\mathrm{Ti_{76}Ni_{24}}) + c(\mathrm{Zr_{76}Ni_{24}}) + d(\mathrm{Hf_{84}Ni_{16}}) \quad (5)$$

The initial mixing constants, a, b, c and d, may then be calculated by substituting the heat of mixing for each of these atomic pairs into Eq. (4), corresponding to $a = 0.60$, $b = 0.16$, $c = 0.11$ and $d = 0.13$. Thus, a composition of $Ti_{28.36}Cu_{43.8}Ni_{8.56}Zr_{8.36}Hf_{10.92}$ is developed. At the calculated composition, the high contents of Zr and Hf elements would result in a high cost, and hence a reduction in the contents of these two elements would be desirable. Therefore, using values of $c = 0.10$ and $d = 0.10$, corresponding values of $a = 0.64$ and $b = 0.16$ are obtained, yielding a composition of $Ti_{29.44}Cu_{46.72}Ni_{7.84}Zr_{7.6}Hf_{8.4}$. Since a high content of Cu leads to a large mass density, it is favorable to increase the content of Ti (with the smallest mass density) in a new alloy. Thus, a reduction in the coefficient of the $Ti_{27}Cu_{73}$ deep eutectic unit, and an increase in the $Ti_{76}Ni_{24}$ unit are required. Therefore, in the present study, the deep eutectic units in the novel Ti–Cu–Ni–Zr–Hf alloys were formulated as:

$$C_{am} = (0.64 - x)(\mathrm{Ti_{27}Cu_{73}}) + (0.16 + x)(\mathrm{Ti_{76}Ni_{24}}) + 0.1(\mathrm{Zr_{76}Ni_{24}}) + 0.1(\mathrm{Hf_{84}Ni_{16}}) \quad (6)$$

Table 1
The enthalpy of mixing in the Ti–Cu–Ni–Zr–Hf system.

Elements	Enthalpy of mixing (kJ mol^{-1})				
	Ti	Cu	Ni	Zr	Hf
Ti	0	–	–	–	–
Cu	−9	0			
Ni	−35	4	0		
Zr	0	−23	−49	0	
Hf	0	−17	−42	0	0

where $x = 0$, 0.02, 0.04, 0.06 or 0.08. On the basis of Eq. (4), five different types of alloy, i.e., $Ti_{29.44}Cu_{46.72}Ni_{7.84}Zr_{7.6}Hf_{8.4}$ ($x = 0$), $Ti_{30.42}Cu_{45.26}Ni_{8.32}Zr_{7.6}Hf_{8.4}$ ($x = 0.02$), $Ti_{31.4}Cu_{43.8}Ni_{8.8}Zr_{7.6}Hf_{8.4}$ ($x = 0.04$), $Ti_{32.38}Cu_{42.34}Ni_{9.28}Zr_{7.6}Hf_{8.4}$ ($x = 0.06$) and $Ti_{33.36}Cu_{40.88}Ni_{9.76}Zr_{7.6}Hf_{8.4}$ ($x = 0.08$) were prepared.

4. Results and discussion

The XRD patterns of the as-cast Ti–Cu–Ni–Zr–Hf samples, with diameters of 3 mm or 4 mm, are shown in Fig. 1. The XRD pattern of the $Ti_{33.36}Cu_{40.88}Ni_{9.76}Zr_{7.6}Hf_{8.4}$ ($x = 0.08$) alloy, at a diameter of 3 mm, exhibited a small diffraction peak (indexed as a TiNi phase) imposed on the first broad peak, which suggests that some tiny TiNi crystals had precipitated in the amorphous phase matrix. However, the XRD patterns of the other alloys, at a diameter of 3 mm, exhibited two broad diffraction peaks that were typical of that of an amorphous phase (Fig. 1a). When the diameter was increased to 4 mm, the diffraction patterns of the $Ti_{30.42}Cu_{45.26}Ni_{8.32}Zr_{7.6}Hf_{8.4}$ ($x = 0.02$), $Ti_{31.4}Cu_{43.8}Ni_{8.8}Zr_{7.6}Hf_{8.4}$ ($x = 0.04$) and $Ti_{32.38}Cu_{42.34}Ni_{9.28}Zr_{7.6}Hf_{8.4}$ ($x = 0.06$) alloys showed broad peaks without significant crystalline diffraction peaks, indicative of a fully glassy nature. However, the XRD patterns of both the $Ti_{29.44}Cu_{46.72}Ni_{7.88}Zr_{7.6}Hf_{8.4}$ ($x = 0$) and $Ti_{33.36}Cu_{40.88}Ni_{9.76}Zr_{7.6}Hf_{8.4}$ ($x = 0.08$) alloys showed a weak diffraction peak imposed on the first broad peak, indexed as TiCu and TiNi phases, respectively; this indicates that tiny crystals of TiCu and TiNi, respectively, had precipitated in the amorphous phase matrix. The high Cu or Ni contents promote the formation of TiCu or TiNi crystal phases, which were also found in the TiCuNiCo or TiCuNiZr alloys [8,24], respectively. These results show that for the novel Ti–Cu–Ni–Zr–Hf alloys, the critical size for forming a fully amorphous phase can approach 2–4 mm. The GFA of the present alloys is higher than that of the $Ti_{20}Cu_{20}Ni_{20}Zr_{20}Hf_{20}$ alloy with a critical diameter of 1.5 mm [21], and similar to that of the Ti–Cu–Ni–Zr alloys [8,25].

The DSC and DTA traces of the five alloys, at a diameter of 3 mm, are shown in Fig. 2. These data provide the relevant thermal parameters, such as the glass transition temperature, T_g, the crystallization onset temperature, T_x, the melting temperature, T_m, and the liquidus temperature, T_l. The DSC curves of these alloys (see Fig. 2a) exhibited an endothermic event followed by several exothermic peaks, indicating transformation of a metastable supercooled liquid phase to equilibrium crystalline phases. The thermal parameters measured from the DSC and DTA traces for these alloys are listed in Table 2; these parameters include the supercooled liquid region, ΔT_x, the reduced glass transition temperature, T_{rg} [2], the GFA parameter, γ [4], the heat of fusion, ΔH_m, and the entropy of fusion, ΔS_m ($=\Delta H_m/T_m$) at the T_m. The γ values of the $Ti_{29.44}Cu_{46.72}Ni_{7.88}Zr_{7.6}Hf_{8.4}$ and $Ti_{33.36}Cu_{40.88}Ni_{9.76}Zr_{7.6}Hf_{8.4}$ alloys, with a critical diameter of 3 mm, were

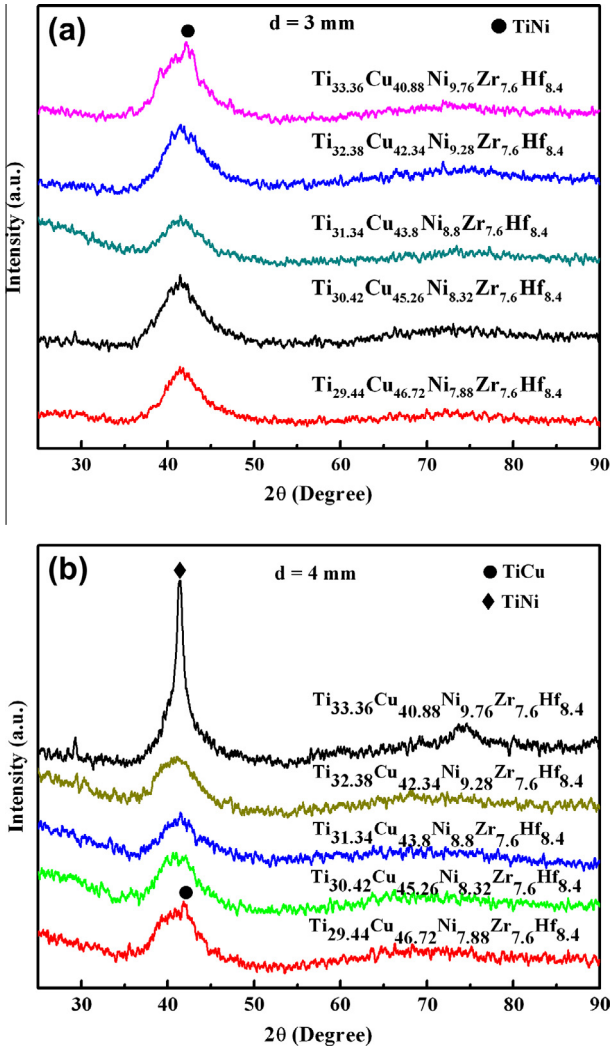

Fig. 1. XRD patterns for the Ti–Cu–Ni–Zr–Hf alloys, taken from rods with diameters of 3 mm or 4 mm.

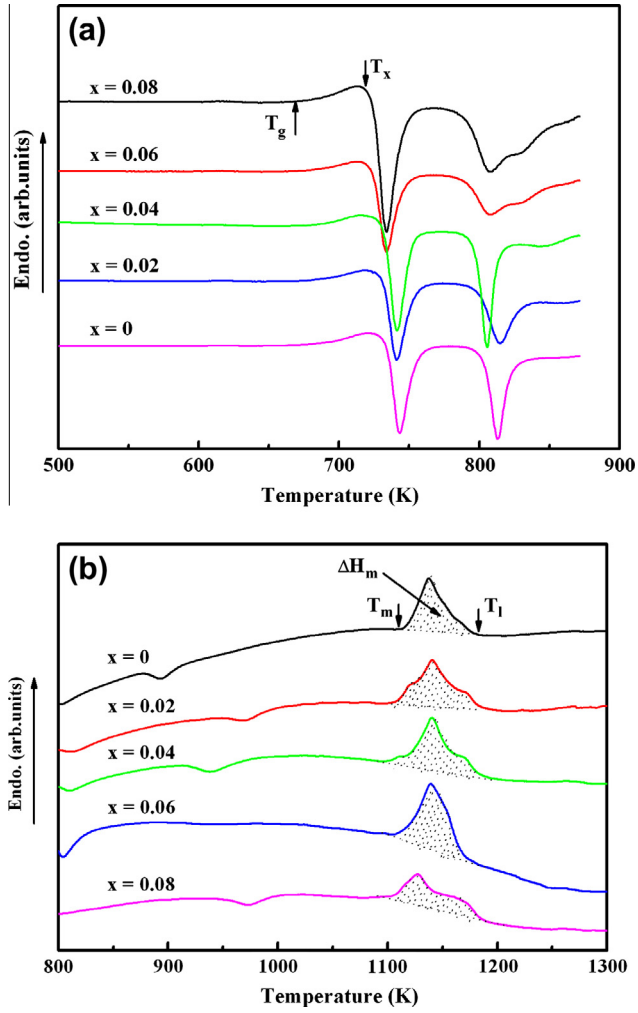

Fig. 2. DSC (a) and DTA (b) traces for the Ti–Cu–Ni–Zr–Hf metallic glasses, with diameters of 3 mm, obtained at a heating rate of 0.33 K s^{-1}.

Table 2
Thermal parameters and the critical diameter, d_c, yield stress, σ_y, and fracture stress, σ_f, of the five Ti–Cu–Ni–Zr–Hf alloys.

Composition	d_c (mm)	T_g (K)	T_x (K)	ΔT_x (K)	T_m (K)	T_l (K)	T_{rg}	ΔH_m (kJ mol^{-1})	ΔS_m (J mol^{-1} K^{-1})	γ	σ_y (MPa)	σ_f (MPa)
$Ti_{29.44}Cu_{46.72}Ni_{7.88}Zr_{7.6}Hf_{8.4}$	3	684	729	45	1099	1195	0.572	11.29	10.28	0.388	2050	2131
$Ti_{30.42}Cu_{45.26}Ni_{8.32}Zr_{7.6}Hf_{8.4}$	4	680	729	49	1105	1189	0.572	11.44	10.35	0.390	2115	2161
$Ti_{31.4}Cu_{43.8}Ni_{8.8}Zr_{7.6}Hf_{8.4}$	4	683	726	44	1115	1185	0.576	11.82	10.60	0.389	2021	2110
$Ti_{32.38}Cu_{42.34}Ni_{9.28}Zr_{7.6}Hf_{8.4}$	4	682	722	39	1111	1168	0.584	11.48	10.34	0.390	2072	2117
$Ti_{33.36}Cu_{40.88}Ni_{9.76}Zr_{7.6}Hf_{8.4}$	<3	679	716	37	1105	1188	0.572	10.01	9.06	0.383	–	–

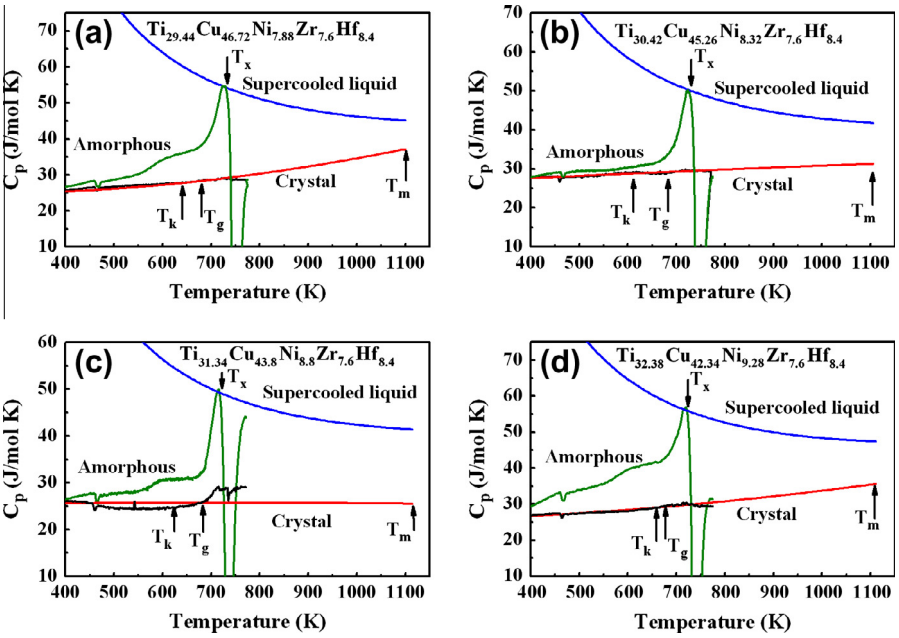

Fig. 3. The specific heat capacity (C_p) of the crystalline solid (black line), the supercooled liquid (the approximately stable C_p values at the smaller temperature range from T_g to T_x in olive line) measured with constant heating rate experiments. The fitting curves of the specific heat capacity for the supercooled liquid (blue line) and crystalline solid (red line) using Eqs. (7) and (8). (For interpretation of the references to color in this figure legend, the reader is referred to the web version of this article.)

Table 3
Fitting parameters for the specific heat data in the crystalline state and supercooled liquid state, together with the ΔC_p^m, $\Delta C_p^m/\Delta S_m$, δ and T_K values for the four alloys.

Parameters	A (J mol^{-1} K^{-2})	B (J mol^{-1} K^{-3})	C (J mol^{-1} K^{-2})	D (J mol^{-1} K^{-2})	ΔC_p^m (J mol^{-1} K^{-1})	$\Delta C_p^m/\Delta S_m$	δ	T_K (K)
$Ti_{29.44}Cu_{46.72}Ni_{7.88}Zr_{7.6}Hf_{8.4}$	−0.005006	1.466×10^{-5}	0.009779	1.1805×10^{7}	8.31	0.81	0.537	643.7
$Ti_{30.42}Cu_{45.26}Ni_{8.32}Zr_{7.6}Hf_{8.4}$	0.007067	-1.231×10^{-6}	0.007483	1.0456×10^{7}	10.53	1.02	0.581	613.1
$Ti_{31.4}Cu_{43.8}Ni_{8.8}Zr_{7.6}Hf_{8.4}$	0.00225	1.5595×10^{-6}	0.0078	9.6489×10^{6}	12.01	1.13	0.601	623.2
$Ti_{32.38}Cu_{42.34}Ni_{9.28}Zr_{7.6}Hf_{8.4}$	0.001289	7.48×10^{-6}	0.01162	1.18×10^{7}	11.81	1.14	0.603	662.2

significantly lower than those of the other alloys, with a critical diameter of 4 mm. It was found that the GFA did not correlate with the temperature range of the supercooled liquid region, ΔT_x, but was slightly related to the T_{rg} value (Table 2), which is consistent with the findings previously reported in La-based [26] and Ce-based [27] BMGs.

The results described above show that modification of the ratios of the binary eutectic units did not obviously change the GFA of the novel Ti–Cu–Ni–Zr–Hf alloys. This will be discussed in the framework of thermodynamics. The Gibbs free energy difference, ΔG, between the supercooled liquid state and the crystalline state is key to elucidating crystal nucleation and growth in the amorphous phase, and can effectively predict the GFA of alloys [28]. The nucleation rate exponentially depends on ΔG, which is believed to be a driving force for crystallization [29]. ΔG can be further investigated by measuring the specific heat of the $Ti_{29.44}Cu_{46.72}Ni_{7.88}Zr_{7.6}Hf_{8.4}$, $Ti_{30.42}Cu_{45.26}Ni_{8.32}Zr_{7.6}Hf_{8.4}$, $Ti_{31.4}Cu_{43.8}Ni_{8.8}Zr_{7.6}Hf_{8.4}$ and $Ti_{32.38}Cu_{42.34}Ni_{9.28}Zr_{7.6}Hf_{8.4}$ alloys. Fig. 3 shows the specific heat values of four alloys at different states, including the crystalline state, amorphous state and supercooled liquid state. The specific heat values of the crystal state and the supercooled liquid state are usually fitted by the following relationships [22,30]:

$$C_p^s = 3R + A \cdot T + B \cdot T^2 \tag{7}$$

$$C_p^l = 3R + C \cdot T + D \cdot T^{-2} \tag{8}$$

where $R = 8.314$ J/g atom^{-1} K^{-1} and A, B, C and D are the fitting parameters. Table 3 lists the fitting results together with the specific heat difference, ΔC_p^m, between the C_p (liquid) and C_p (crystal) at T_m, and the $\Delta C_p^m/\Delta S_m$, δ and T_K values for the four alloys. Based on the experimental data, the enthalpy difference, ΔH, and the entropy difference, ΔS, of the supercooled liquid state with respect to the

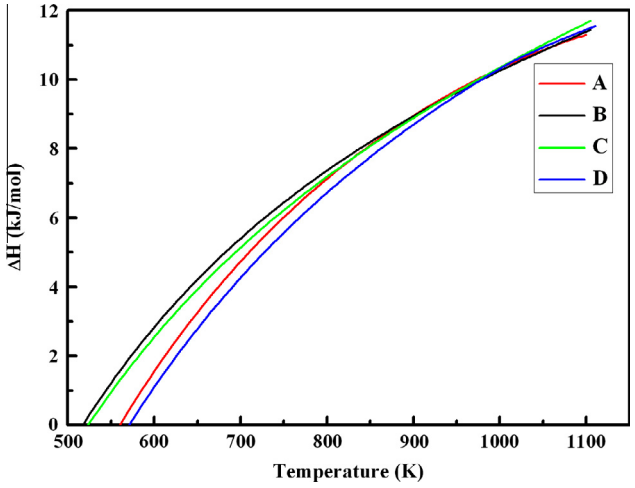

Fig. 4. Enthalpy change (ΔH) of the supercooled liquid with respect to the crystal, for the $Ti_{29.44}Cu_{46.72}Ni_{7.88}Zr_{7.6}Hf_{8.4}$ (A), $Ti_{32.38}Cu_{42.34}Ni_{9.28}Zr_{7.6}Hf_{8.4}$ (B), $Ti_{31.4}Cu_{43.8}Ni_{8.8}Zr_{7.6}Hf_{8.4}$ (C) and $Ti_{32.38}Cu_{42.34}Ni_{9.28}Zr_{7.6}Hf_{8.4}$ (D) alloys.

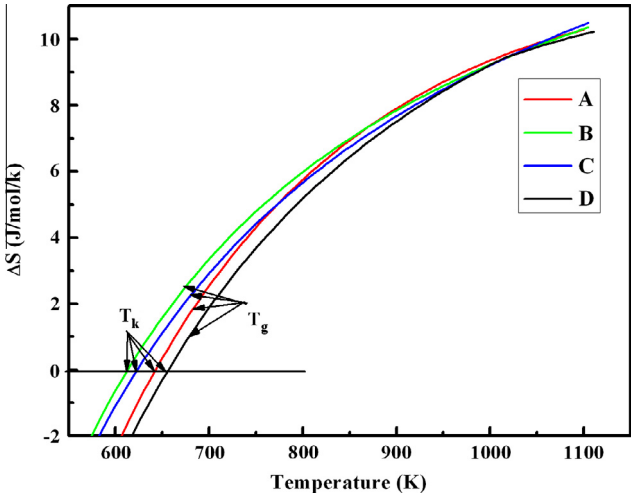

Fig. 5. Entropy change (ΔS) of the supercooled liquid with respect to the crystal, for the $Ti_{29.44}Cu_{46.72}Ni_{7.88}Zr_{7.6}Hf_{8.4}$ (A), $Ti_{32.38}Cu_{42.34}Ni_{9.28}Zr_{7.6}Hf_{8.4}$ (B), $Ti_{31.4}Cu_{43.8}Ni_{8.8}Zr_{7.6}Hf_{8.4}$ (C) and $Ti_{32.38}Cu_{42.34}Ni_{9.28}Zr_{7.6}Hf_{8.4}$ (D) alloys. The Kauzmann temperature (T_K) and glass transition temperature (T_g) for each of the alloys are indicated by arrows in the plots.

crystal state, may be calculated according to the following equations:

$$\Delta H = \Delta H_m - \int_T^{T_m} (C_P^l - C_p^s) dT \tag{9}$$

$$\Delta S = \Delta S_m - \int_T^{T_m} \frac{C_P^l - C_p^s}{T} dT \tag{10}$$

The results are plotted in Figs. 4 and 5. It is evident that the enthalpy of the supercooled liquid decreases more slowly than the entropy, which leads to an entropy crisis at the Kauzmann temperature, T_K. The T_K represents the lowest temperature at which a supercooled liquid can exist [29], where $\Delta S = 0$ or the entropy of the liquid equals that of the crystalline state. In the present study, the calculated T_K values were 644 K for the $Ti_{29.44}Cu_{46.72}Ni_{7.88}Zr_{7.6}Hf_{8.4}$ alloy, 613 K for the $Ti_{30.42}Cu_{45.26}Ni_{8.32}Zr_{7.6}Hf_{8.4}$ alloy, 623 K for the $Ti_{31.4}Cu_{43.8}Ni_{8.8}Zr_{7.6}Hf_{8.4}$ alloy and 662 K for the $Ti_{32.38}Cu_{42.34}Ni_{9.28}Zr_{7.6}Hf_{8.4}$ alloy.

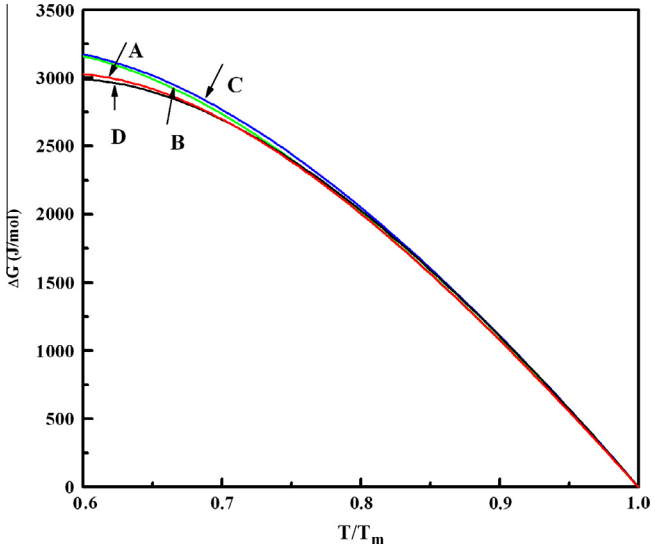

Fig. 6. Gibbs free energy difference (ΔG) of the supercooled liquid with respect to the crystal, for the $Ti_{29.44}Cu_{46.72}Ni_{7.88}Zr_{7.6}Hf_{8.4}$ (A), $Ti_{32.38}Cu_{42.34}Ni_{9.28}Zr_{7.6}Hf_{8.4}$ (B), $Ti_{31.4}Cu_{43.8}Ni_{8.8}Zr_{7.6}Hf_{8.4}$ (C) and $Ti_{32.38}Cu_{42.34}Ni_{9.28}Zr_{7.6}Hf_{8.4}$ (D) alloys.

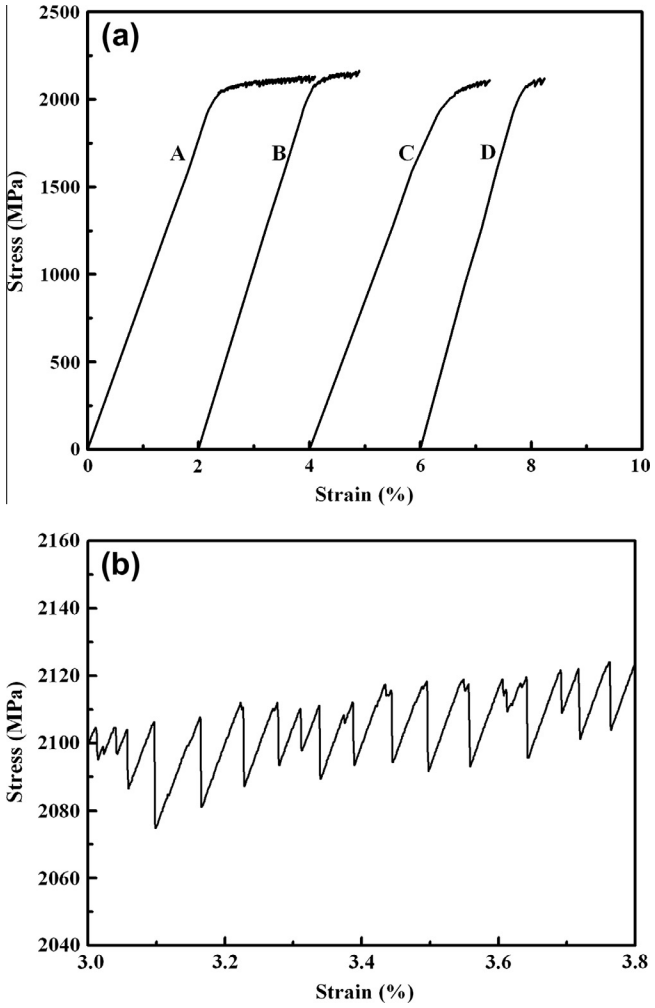

Fig. 7. Compressive stress–strain curves for as-cast glassy rods (2 mm in diameter and ~4 mm in length) obtained at a strain rate of $2.5 \times 10^{-4}\,s^{-1}$ at room temperature. Curves are shown for the $Ti_{29.44}Cu_{46.72}Ni_{7.88}Zr_{7.6}Hf_{8.4}$ (A), $Ti_{30.42}Cu_{45.26}Ni_{8.32}Zr_{7.6}Hf_{8.4}$ (B), $Ti_{31.4}Cu_{43.8}Ni_{8.8}Zr_{7.6}Hf_{8.4}$ (C) and $Ti_{32.38}Cu_{42.34}Ni_{9.28}Zr_{7.6}Hf_{8.4}$ (D) alloys.

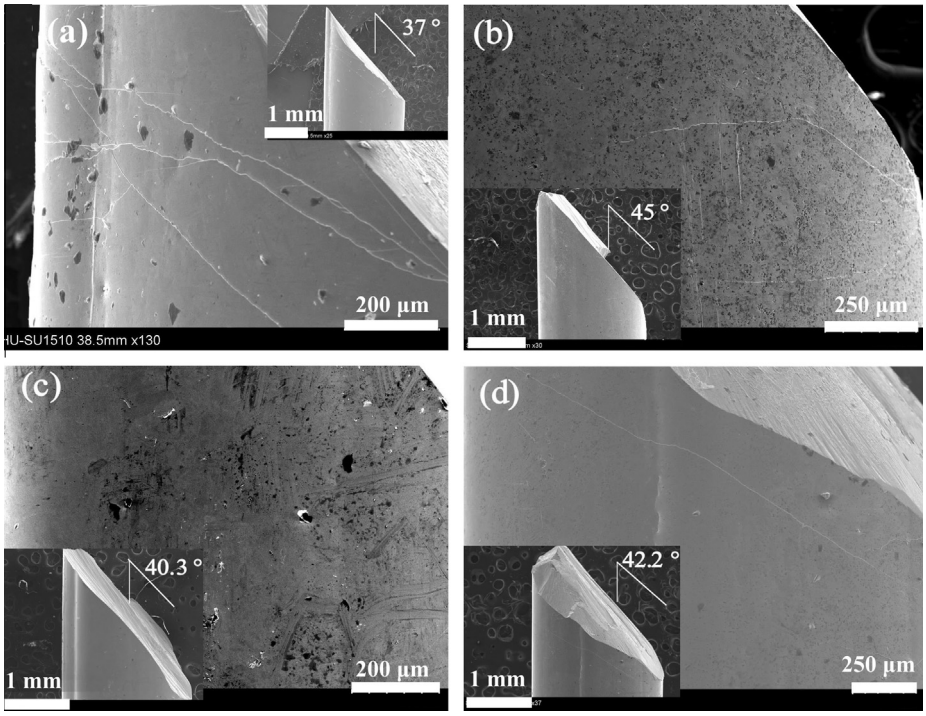

Fig. 8. SEM images showing side-views of the fractured samples. (a) $Ti_{29.44}Cu_{46.72}Ni_{7.88}Zr_{7.6}Hf_{8.4}$, (b) $Ti_{30.42}Cu_{45.26}Ni_{8.32}Zr_{7.6}Hf_{8.4}$, (c) $Ti_{31.4}Cu_{43.8}Ni_{8.8}Zr_{7.6}Hf_{8.4}$ and (d) $Ti_{32.38}Cu_{42.34}Ni_{9.28}Zr_{7.6}Hf_{8.4}$. The insets show the fractured pieces and the fracture angles of the samples.

The Gibbs free energy difference, ΔG, may be calculated as:

$$\Delta G = \Delta H - \Delta S \cdot T \tag{11}$$

The Gibbs free energy differences, as a function of the temperature normalized to the melting temperature, for the four alloys, are plotted in Fig. 6. The highest ΔG value (3.143 kJ mol^{-1} at T_g) occurs in the $Ti_{31.4}Cu_{43.8}Ni_{8.8}Zr_{7.6}Hf_{8.4}$ alloy (Fig. 6), which has a relatively high GFA (Table 2). The $Ti_{29.44}Cu_{46.72}Ni_{7.88}Zr_{7.6}Hf_{8.4}$ alloy, which has a relative low GFA, exhibits the lowest ΔG value (2.973 kJ mol^{-1} at T_g). However, since the differences between the free energy curves for the four alloys are small, the GFA of these four alloys are similar. Based on the hole theory of liquids, the high values of δ and $\Delta C_p^m/\Delta S_m$ suggest a low critical cooling rate for amorphous formation in liquids, i.e., a good GFA [28]. The correlation between the GFA parameter, δ, and $\Delta C_p^m/\Delta S_m$ for BMGs may be shown as [28]:

$$\delta = \left[\frac{\Delta C_p^m/\Delta S_m}{2 + \Delta C_p^m/\Delta S_m}\right]^{1/2} \tag{12}$$

The δ and $\Delta C_p^m/\Delta S_m$ values for the $Ti_{29.44}Cu_{46.72}Ni_{7.88}Zr_{7.6}Hf_{8.4}$ alloy are 0.537 and 0.81, respectively, the lowest among the four alloys (Table 3), indicating that the δ and $\Delta C_p^m/\Delta S_m$ values can effectively reflect the GFA of the present Ti–Cu-based alloys.

The nominal compressive stress–strain curves for the four BMGs are shown in Fig. 7a. All the BMGs displayed similar elastic deformation but different plastic deformation prior to failure. Of these four BMGs, the $Ti_{29.44}Cu_{46.72}Ni_{7.88}Zr_{7.6}Hf_{8.4}$ BMG showed excellent mechanical properties, such as a large plastic strain of 1.8%, and a high fracture strength of 2131 MPa. This fracture strength is higher than that of 1920 MPa for $Ti_{20}Cu_{20}Ni_{20}Zr_{20}Hf_{20}$ BMG [21], and that of 2100 MPa for Ti–Cu–Zr–Pd MG annealed at 693 K [17]. The other BMGs exhibited lower deformability at room temperature. The yield and fracture stresses of the alloys are summarized in Table 2. The plasticity for the $Ti_{29.44}Cu_{46.72}Ni_{7.88}Zr_{7.6}Hf_{8.4}$ BMG is further confirmed by the serrated flow in the plastic region of the stress–strain curve in Fig. 7b. Plastic deformation in BMGs is associated with a multiplication of shear bands [31–33] and numerous fine shear bands [34]. This was further verified by SEM observations. Fig. 8a displays typical, multiple and fine shear bands at the external surfaces of the $Ti_{29.44}Cu_{46.72}Ni_{7.88}Zr_{7.6}Hf_{8.4}$ BMG. The external surfaces of the other three BMGs showed one or two shear bands (Fig. 8b–d), consistent with the low plastic strain evident in Fig. 7a. The insets in Fig. 8 illustrate that final fracture of the alloy occurred along the maximal shear stress plane, which was inclined to the direction of the load. The shear fracture angles for the four alloys with respect to the loading direction were 37°, 45°, 40.3° and 42.2°. The results agree well with previous observations for other BMGs [31,32], indicating that deformation of the BMGs in this study satisfied the Mohr–Coulomb criterion [35,36].

5. Conclusions

The pentabasic Ti–Cu–Ni–Zr–Hf BMGs without noble elements and poisonous elements were successfully developed, which exhibited relative high GFA because their maximum critical diameter approaches 3 and 4 mm. Among this alloy system, the $Ti_{29.44}Cu_{46.72}Ni_{7.88}Zr_{7.6}Hf_{8.4}$ alloy had a lower GFA, and exhibited favorable mechanical properties, i.e., a high fracture strength of 2131 MPa and a pronounced plastic strain of 1.8%. The thermodynamic calculation based on the hole theory of the liquid state found that the smallest reduced ideal glass transition temperature and the ratio of $\Delta C_p^m/\Delta S_m$ happen in the $Ti_{29.44}Cu_{46.72}Ni_{7.88}Zr_{7.6}Hf_{8.4}$ alloy, confirming that this alloy has the poor GFA. The fractographic observation showed the multiple and fine shear bands at the external surfaces of the $Ti_{29.44}Cu_{46.72}Ni_{7.88}Zr_{7.6}Hf_{8.4}$ BMG, which was the possible reason resulting in the relative good plasticity.

Acknowledgement

This work was supported by the National Natural Science Foundation of China (NSFC) under Grant No. 51025415.

References

[1] Edwards KL, Axinte E, Tabacaru LL. A critical study of the emergence of glass and glassy metals as "green" materials. Mater Des 2013;50:713–23.
[2] Turnbull D. Under what conditions can a glass be formed? Contemp Phys 1969;10:473–88.
[3] Inoue A. Stabilization of metallic supercooled liquid and bulk amorphous alloys. Acta Mater 2000;48:279–306.
[4] Lu ZP, Liu CT. A new glass-forming ability criterion for bulk metallic glasses. Acta Mater 2002;50:3501–12.
[5] Ji XL, Pan Y, Ni FS. A thermodynamic criterion for predicting glass-forming ability in binary metallic glasses. Mater Des 2009;30:842–5.
[6] Hao GJ, Lin JP, Zhang Y, Chen GL, Lu ZP. Ti–Zr–Be ternary bulk metallic glasses correlated with binary eutectic clusters. Mater Sci Eng A 2010;527:6248–50.
[7] Shen J, Zou J, Ye L, Lu ZP, Xing DW, Yan M. Glass-forming ability and thermal stability of a new bulk metallic glass in the quaternary Zr–Cu–Ni–Al system. J Non-Cryst Solids 2005;351:2519–23.
[8] Lu ZP, Shen J, Xing DW, Sun JF, Liu CT. Binary eutectic clusters and glass formation in ideal glass-forming liquids. Appl Phys Lett 2006;89:071910-1–0-3.
[9] Sun YJ, Qu DD, Huang YJ, Liss KD, Wei XS, Xing DW, et al. Zr–Cu–Ni–Al bulk metallic glasses with superhigh glass-forming ability. Acta Mater 2009;57:1290–9.
[10] Yang YJ, Xing DW, Li CP, Wei SD, Sun JK, Shen QK. A new way of designing bulk metallic glasses in Cu–Ti–Zr–Ni system. Mater Sci Eng A 2007;448:15–9.
[11] Li PY, Wang G, Ding D, Shen J. Glass forming ability and thermodynamics in the new Ti–Cu–Ni–Zr bulk metallic glasses. J Non-Cryst Solids 2012; 358:3200–4.
[12] Kim YC, Na JH, Park JM, Kim DH, Lee YH, Kim WT. Role of nanometer-scale quasicrystals in improving the mechanical behavior of Ti-based bulk metallic glasses. Appl Phys Lett 2003;83:3093–5.
[13] Wiest A, Duan G, Demetriou MD, Wiest LA, Peck A, Kaltenboeck G, et al. Zr–Ti-based Be-bearing glasses optimized for high thermal stability and thermoplastic formability. Acta Mater 2008;56:2625–30.
[14] Bae DH, Park JM, Na JH, Kim DH, Kim YC, Lee JK. Deformation behavior of Ti–Zr–Ni–Cu–Be metallic glass and composite in the supercooled liquid region. J Mater Res 2004;19:937–42.
[15] Duan G, Wiest A, Lind M, Kahl A, Johnson WL. Lightweight Ti-based bulk metallic glasses excluding late transition metals. Scripta Mater 2008;58:465–8.
[16] Qin FX, Wang XM, Inoue A. Effect of annealing on microstructure and mechanical property of a Ti–Zr–Cu–Pd bulk metallic glass. Intermetallics 2007;15:1337–42.
[17] Zhu SL, Wang XM, Qin FX, Yoshimura M, Inoue A. New TiZrCuPd quaternary bulk glassy alloys with potential of biomedical applications. Mater Trans 2007;48:2445–8.
[18] Oak JJ, Louzguine-Luzgin DV, Inoue A. Fabrication of Ni-free Ti-based bulk-metallic glassy alloy having potential for application as biomaterial, and investigation of its mechanical properties, corrosion, and crystallization behavior. J Mater Res 2007;22:1346–53.
[19] Louzguine DV, Inoue A. Nanocrystallization of Ti–Ni–Cu–Sn amorphous alloy. Scripta Mater 2000;43:371–6.
[20] Men H, Pang SP, Inoue A, Zhang T. New Ti-based bulk metallic glasses with significant plasticity materials transactions. Mater Trans 2005;46:2218–20.
[21] Ma LQ, Wang LM, Zhang T, Inoue A. Bulk glass formation of Ti–Zr–Hf–Cu–M (M = Fe, Co, Ni) alloys. Mater Trans 2002;43:277–80.
[22] Busch R, Kim YJ, Johnson WL. Thermodynamics and kinetics of the undercooled liquid and the glass transition of the $Zr_{41.2}Ti_{13.8}Cu_{12.5}Ni_{10.0}Be_{22.5}$ alloy. J Appl Phys 1995;77:4039–43.
[23] Takeuchi A, Inoue A. Classification of bulk metallic glasses by atomic size difference, heat of mixing and period of constituent elements and its application to characterization of the main alloying element. Mater Trans 2005;12:2817–29.
[24] Wang G, Huang YJ, Shen J. Novel TiCuNiCo composites with high fracture strength and plasticity. Mater Des 2012;33:226–30.
[25] Lin XH, Johnson WL. Formation of Ti–Zr–Cu–Ni bulk metallic glasses. J Appl Phys 1995;78:6514–9.
[26] Li PY, Li SD, Tian ZJ, Huang ZG, Zhang FM, Du YW. Effect of Ni–Al atomic ratio on glass formation in La–Al–Cu–Ni bulk metallic glasses. J Alloys Compd 2009;478:193–6.
[27] Zhang B, Wang RJ, Zhao DQ, Pan MX, Wang WH. Superior glass-forming ability through microalloying in cerium-based alloys. Phys Rev B 2006;73:092201-1–1-4.
[28] Singh PK, Dubey KS. Thermodynamic behaviour of bulk metallic glasses. Thermochim Acta 2012;530:120–7.
[29] Eckler K, Herlach DM. Measurements of dendrite growth Ni-melts some new results. Mater Sci Eng A 1994;178:159–62.
[30] Lu ZP, Li Y, Liu CT. Glass-forming tendency of bulk La–Al–Ni–Cu–(Co) metallic glass-forming liquids. J Appl Phys 2003;93:286–90.
[31] Wright WJ, Saha WR, Nix WD. Deformation mechanisms of the $Zr_{40}Ti_{14}Ni_{10}Cu_{12}Be_{24}$ bulk metallic glass. Mater Trans 2001;42:642–9.
[32] Song SX, Bei H, Wadsworth J, Nieh TG. Flow serration in a Zr-based bulk metallic glass in compression at low strain rates. Intermetallics 2008;16:813–8.
[33] Sun BA, Pauly S, Tan J, Stoica M, Wang WH, Kühn U, et al. Serrated flow and stick-slip deformation dynamics in the presence of shear-band interactions for a Zr-based metallic glass. Acta Mater 2012;60:4160–71.
[34] Xue YF, Wang L, Cheng XW, Wang FC, Cheng HW, Zhang HF, et al. Strain rate dependent plastic mutation in a bulk metallic glass under compression. Mater Des 2012;36:284–8.
[35] Zhang ZF, He G, Zhang H, Eckert J. Rotation mechanism of shear fracture induced by high plasticity in Ti-based nano-structured composites containing ductile dendrites. Scripta Mater 2005;52:945–9.
[36] Zhang ZF, Eckert J. Unified tensile fracture criterion. Phys Rev Lett 2005;94:094301–94304.